Numerical analysis of an electromagnetic energy harvester driven by multiple magnetic forces under pulse excitation

Dibin Zhu and Lawrence Evans

College of Mathematics, Engineering and Physical Sciences, University of Exeter, Exeter UK, EX4 4QF

E-mail: d.zhu@exeter.ac.uk

Abstract

This paper presents a numerical analysis model for an electromagnetic energy harvester that is driven by multiple magnetic forces under pulse excitation. The energy harvester consists of a tube with magnets on both ends and a shuttle magnet moving inside. It converts pulse excitation to oscillation of the shuttle magnet with higher frequency and amplitude. A numerical model was developed to model operation of the energy harvester. The model correlates analytical calculation of magnetic forces and simulation results of magnetic field in Maxwell. Operation of the structure was then analysed using fundamental equations of motion in the time domain. A prototype was fabricated and two example scenarios were tested to verify the numerical model. Experimental results in both scenarios were found to agree with results obtained from the numerical analysis. It was also found in the numerical analysis that initial positions of the end magnets with respect to the shuttle magnet are crucial to the performance of the energy harvester. If the distance between the end magnet and the shuttle magnet reduces, oscillation of the shuttle magnet will last longer but have smaller amplitude. If such distance reduces below a threshold, the shuttle magnet cannot move at all. Furthermore, friction between the shuttle magnet and the tube also affects its oscillation. The lower the friction becomes, the longer the oscillation can last and the higher the oscillation amplitude can be.

Keywords: numerical analysis, energy harvesting, electromagnetic, pulse excitation

---

1. Introduction

Energy harvesting from pulse excitation such as footsteps has drawn a lot of attention in recent years [1][2][3]. It enables electrical energy to be generated while one is walking or running. Applications of such technology ranges widely from powering wearable electronic devices [4] to powering streetlights [5]. One of the major challenges of harvesting energy from pulse excitation is that input force in such applications normally has low frequency, e.g. ~1 Hz for walking and < 5Hz for running. Fundamental analysis of kinetic energy harvesting suggests that more mechanical power is available to be harvested if the operating frequency is higher and the resonant frequency of the kinetic energy harvester matches it [6]. This makes it difficult to harvest energy harvest from such low frequency excitation. However, energy harvesting from footsteps does benefit from large input forces, which makes it still attractive as an alternative power source for various applications.

Typically, two transducers are used to harvest energy from footsteps, i.e. piezoelectric and electromagnetic. In the piezoelectric method, piezoelectric materials can be applied where stress and strain are produced by the footsteps, such as shoe insole. The change in strain on the piezoelectric materials results in electric charges being generated. By collecting generated charges using electrodes, electric current can be generated. In order to increase the output power of the piezoelectric transducers under pulse excitation, novel structures were proposed to increase the strain applied to the piezoelectric materials including cymbal [7][8] and pre-stressed diaphragm [9]. In such energy harvesters, traditional piezoelectric materials, e.g. PZT, were used. However, PZT are rigid and brittle, which makes it not ideal for applications where input pulse force is large. Therefore, flexible materials that have piezoelectric properties have been investigated to tackle this problem. Luo *et al* [4] reported energy harvesting from footsteps by mounting porous polypropylene, a lightweight ferrelectret material on shoe insole. An average energy of over 100 μJ was generated by each footstep and this is sufficient to power a commercial ZigBee transmitter. In terms of electromagnetic method, the excitation force from footsteps drives a magnet to move with respect to a coil where current is induced. Ylli *et al* [10] presented two electromagnetic energy harvesters for human foot movement. They targeted swing movement and impact during human walking and average power of 0.84 mW and 4.13 mW were achieved by these two harvesters respectively.

Frequency up-conversion method is frequently used to improve output power of energy harvesters under low frequency and pulse excitation [11][12][13]. In this method, two mechanical structures, typically cantilevers, with different resonant frequencies are coupled. The structure with the lower resonant frequency is tuned to match the frequency of ambient excitation and thus resonates under such excitation. Oscillation of this structure then triggers oscillation of the structure with higher resonant frequency where transducer is attached. Therefore, output of an energy harvester with frequency up-conversion has higher frequency compared to the excitation frequency. Consequently, higher output power can be achieved under low frequency excitation. Another solution was proposed by authors of this paper [14]. It converts pulse excitation to higher frequency oscillation with larger amplitude to improve output power. The energy harvester consists of four magnets that interact with each other. The magnets are arranged so that the pulse excitation drives a shuttle to oscillate in a tube with higher frequency and displacement. However, the complexity of the mechanical structure in [14] makes it difficult to be modelled analytically. As multiple magnets are involved, the system is highly nonlinear. Therefore, complete simulation of such a structure in finite element analysis software, such ANSYS and COMSOL, becomes very complicated.

In this paper, a numerical analysis model that correlates analytical and simulation results to describe mechanical operation of the proposed structure in [14] is presented. Performance of the mechanical structure can thus be analysed numerically in the time domain. The proposed model focuses mainly on the mechanical domain. The paper is structured as follows: section 2 will introduce the operation principle of the mechanism. Section 3 will present the numerical model. Section 4 presents and compares numerical results and experimental results followed by discussions and conclusions in Section 5.

2. Principle

The structure of the proposed energy harvester is illustrated in Figure 1. It consists of a cylinder tube with a coil wound around it. A shuttle magnet can travel back and forth inside the tube so that electric current is induced in the coil. One magnet is fixed to one end of the tube to provide repulsive force when the shuttle magnet approaches (the magnet on the left of the tube as in Figure 1(a)). A complementary magnet set (CMS) is suspended by a mechanical spring on the other side of the tube. The CMS consists of two bar magnets with opposite poles facing the end of the tube.

Figure 1(a) shows the original position of the CMS without external force. In this case, the magnet in the CMS that is aligned with the tube has opposite magnetic pole facing the shuttle magnet. Thus, the shuttle magnet moves towards the CMS due to the attractive force between them. When an external force is applied to the CMS as shown in Figure 1(b), the CMS moves downwards and the other magnet in the CMS is aligned with the tube. In this case, there is a repulsive force between the shuttle magnet and the CMS. This causes the shuttle magnet to move away from the CMS. When the shuttle magnet approaches the fixed magnet on the left, the repulsive force pushes it back towards the CMS where it once again encounters the repulsive force from the CMS and thus a higher frequency oscillation is produced. When the external force is released, the CMS returned to its original position thanks to the spring and the shuttle magnet moves back to its original position.

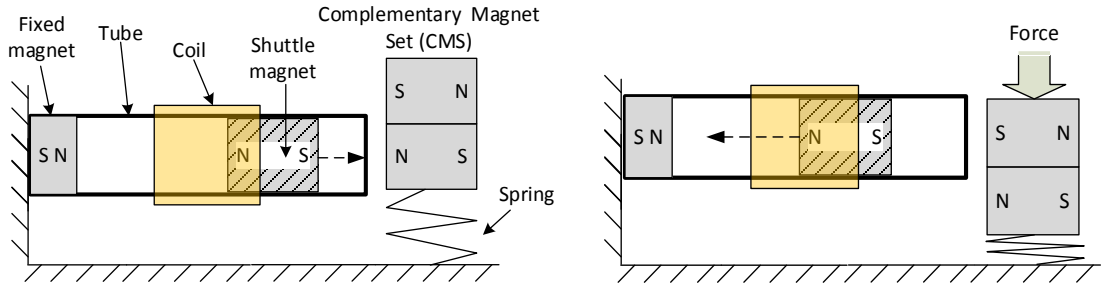

Figure 1. Schematic of the electromagnetic frequency up-converting energy harvester. (a) no external force (b) external force is applied.

Movement of the shuttle magnet is highly nonlinear as it depends on its interaction with other three magnets. This also makes modelling this structure using analytical method very complicated. Therefore, in this study, a numerical method is develop to model operation of this device.

3. Numerical analysis

3.1. Calculation of magnetic force between two magnets

The numerical method to calculate magnetic force between simple shape magnets was reported by Akoun and Yonnet [15]. Figure 2 shows two cubic magnets whose centres are o and o', respectively.

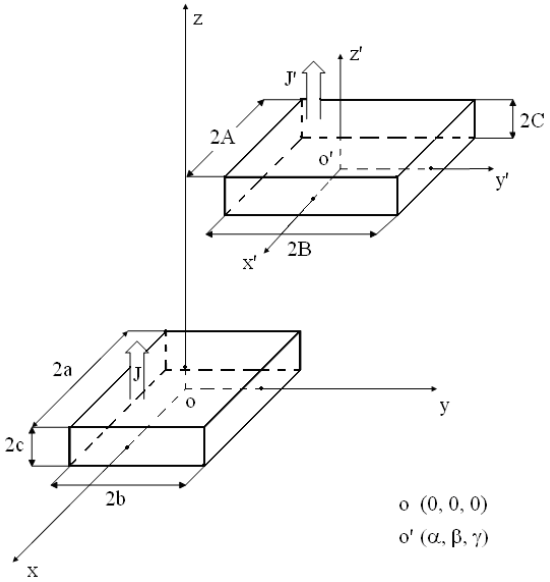

Figure 2. Magnet configuration as used to analytically calculate magnetic force between two magnets.

Their sides are respectively parallel and they are separated by α, β and γ in x, y and z direction (centre to centre), respectively. The dimensions of the lower magnet are 2a × 2b × 2c and that of the upper one is 2A × 2B × 2C. The magnetisations of the two magnets, J and J' are uniform. Their magnetizations are in the z-axis. The magnetic force between these two permanent magnets can be calculated using the following equations [15]:

$$F(\alpha,\beta,\gamma) = \frac{J\cdot J'}{4\pi\mu_0}\sum_{i=0}^{1}\sum_{j=0}^{1}\sum_{k=0}^{1}\sum_{l=0}^{1}\sum_{p=0}^{1}\sum_{q=0}^{1}(-1)^{i+j+k+l+p+q}\cdot\Phi\left(u_{ij},v_{kl},w_{pg},r\right) \qquad (1)$$

For the magnetic force in the x axis, F_x,

$$\Phi_x = \frac{1}{2}\left(v_{ij}^2 - w_{pq}^2\right)\cdot \ln\left(r - u_{ij}\right) + u_{ij}\cdot v_{kl}\cdot \ln\left(r - v_{kl}\right) + v_{kl}\cdot w_{pq}\cdot \tan^{-1}\frac{u_{ij}\cdot v_{kl}}{r\cdot w_{pq}} + \frac{1}{2}r\cdot u_{ij}$$

For the magnetic force in the y axis, F_y,

$$\Phi_y = \frac{1}{2}\left(u_{ij}^2 - w_{pq}^2\right)\cdot \ln\left(r - v_{kl}\right) + u_{ij}\cdot v_{kl}\cdot \ln\left(r - u_{ij}\right) + u_{ij}\cdot w_{pq}\cdot \tan^{-1}\frac{u_{ij}\cdot v_{kl}}{r\cdot w_{pq}} + \frac{1}{2}r\cdot v_{kl}$$

For the magnetic force in the z axis, F_z,

$$\Phi_z = -u_{ij}\cdot w_{pq}\cdot \ln\left(r - u_{ij}\right) - v_{kl}\cdot w_{pq}\cdot \ln\left(r - v_{kl}\right) + u_{ij}\cdot v_{kl}\cdot \tan^{-1}\frac{u_{ij}\cdot v_{kl}}{r\cdot w_{pq}} - r\cdot w_{pq}$$

where

$$u_{ij} = \alpha + (-1)^j A - (-1)^i a$$

$$v_{kl} = \beta + (-1)^l B - (-1)^k b$$

$$w_{pq} = \gamma + (-1)^q C - (-1)^p c$$

$$r = \sqrt{u_{ij}^2 + v_{kl}^2 + w_{pq}^2}$$

Although this method was developed to calculate magnetic force between two cubic magnets, it was found that it can also be used to predict magnetic force between a cylinder magnet and a cubic magnet as required in this work with high accuracy. Simulation was conducted in Maxwell 16.0 to verify this. The simulation model is shown in Figure 3. Dimensions of the cubic magnet are 15 × 15 × 5 mm^3. The cylinder magnet has the diameter of 15 mm and length of 20 mm. Both magnets have identical magnetization which is parallel to the z axis. The two magnets are perfectly aligned along the z axis. In the simulation, magnetic forces between the two magnets were calculated as the distance between them, *d*, varied.

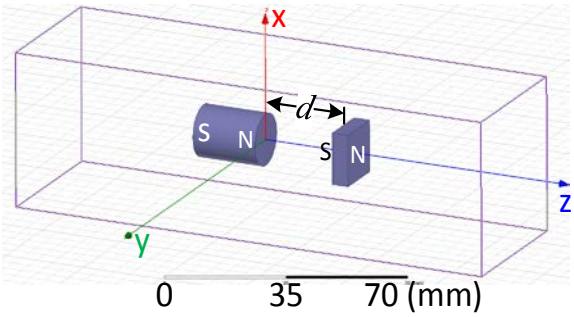

Figure 3. Maxwell model to calculate magnetic force between two magnets.

As a comparison, magnetic forces were also calculated using the analytical method as described in Eq (1). In the analytical calculation, two cubic magnets were considered. One magnet has identical dimensions as the cubic magnet in the Maxwell simulation, i.e. 15 × 15 × 5 mm^3. The other magnet has the same length as the cylinder magnet as in the simulation, i.e. 20 mm. Instead of having a circular cross section, it has a square cross section with the side length of 15 mm each, i.e. same as the diameter of the cylinder magnet.

Figure 4 compares the analytical results of the magnetic force between two cubic magnets and the simulation results of the magnetic force between a cubic magnet and a cylinder magnet. It was found that these results agree with each other very closely. Therefore, the analytical model as described in Eq (1) will be used to calculate magnetic forces between cubic and cylinder magnets in this study.

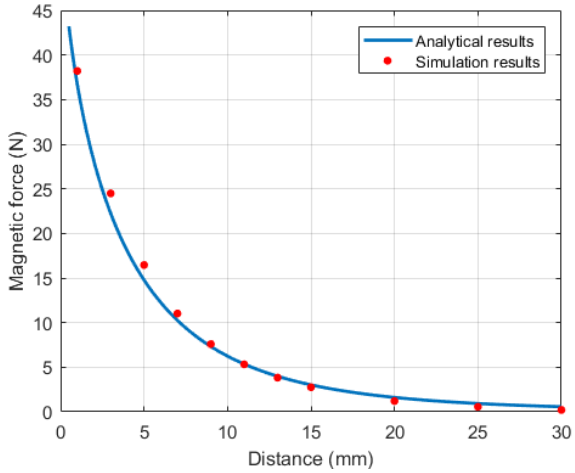

Figure 4. Comparison of analytical and simulation results of magnetic force between two magnets.

3.2. Force analysis of the shuttle magnet

The shuttle magnet in the tube interacts with three other magnets during its movement. Therefore, it always has three sets of magnetic forces applied on it. As all magnets are symmetric with respect to the xz plane, the magnetic force in y direction can be neglected and only magnetic forces in x and z directions are considered in this study. Therefore, force analysis can be simplified to a 2D problem as shown in Figure 5.

In z direction, the three magnetic forces applied to the shuttle magnets are: the repelling force from magnet 1, F_{z1} in –z direction, the repelling force from magnet 2, F_{z2} in +z direction and the attractive force from magnet 3, F_{z3} in –z direction. Therefore, the total magnetic force the shuttle magnet sees in z direction, F_{zTm} is given by:

$$F_{zTm} = F_{z2} - F_{z1} - F_{z3} \tag{2}$$

In x direction, the shuttle magnet is under two magnetic forces from magnets 2 and 3 plus the gravity. The shuttle magnet and magnet 1 aligns perfectly along z direction so the magnetic force between in x direction them can be neglected. There are three possible scenarios in x direction. When the centre of magnet 3 is above the centre of the shuttle magnet, i.e. scenario 1 as shown in Figure 5(a), magnet 3 applies an attractive force, F_{x3}, in –x direction and magnet 2 applies a repelling force, F_{x2}, in +x direction to the shuttle magnet, respectively. When the centre of shuttle magnet is between those of magnets 2 and 3, scenario 2 as shown in Figure 5(b), both magnets 2 and 3 apply a repelling force, F_{x2} and F_{x3}, respectively, in +x direction to the shuttle magnet. When the centre of magnet 2 is below the centre of the shuttle magnet, scenario 3 as shown in Figure 5(c), magnet 3 applies an attractive force, F_{x3}, in +x direction and magnet 2 applies a repelling force, F_{x2}, in –x direction to the shuttle magnet, respectively. Therefore, the total force applied to the shuttle magnet in x direction, F_{xT} is given by:

$$\text{Scenario 1: } F_{xT} = G + F_{x2} - F_{x3} \tag{3}$$
$$\text{Scenario 2: } F_{xT} = G + F_{x2} + F_{x3} \tag{4}$$
$$\text{Scenario 3: } F_{xT} = G - F_{x2} + F_{x3} \tag{5}$$

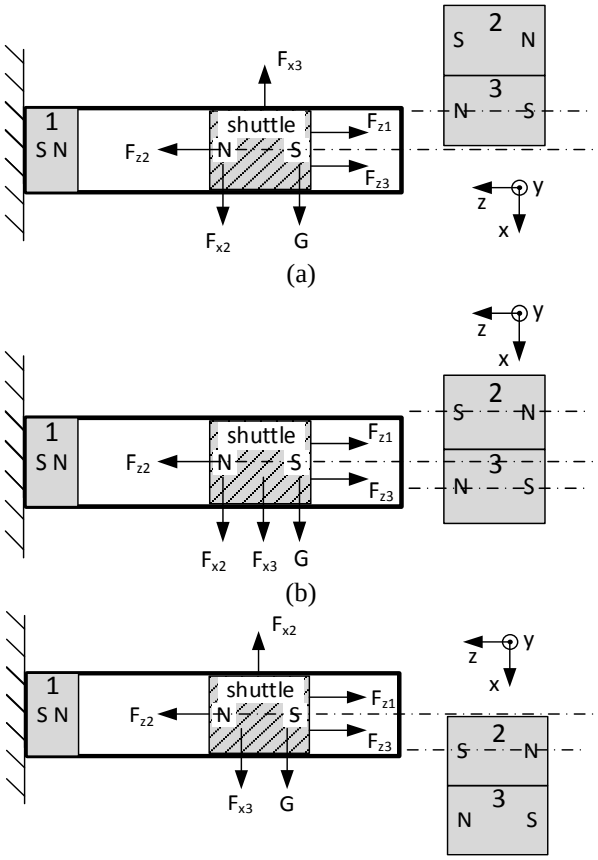

Figure 5. Magnetic forces applied to the shuttle magnet (a) scenario 1 (b) scenario 2 (c) scenario 3.

As the shuttle magnet only moves in z direction, total force in x direction, F_{xT}, which is perpendicular to z direction can be used to calculate the friction as:

$$F_{fr} = \mu \cdot F_{xT} \tag{6}$$

where μ is the coefficient of friction.

The friction is always exerted in a direction that opposes movement (for kinetic friction) or potential movement (for static friction) between the shuttle magnet and the tube. Therefore, when the shuttle magnet moves or tends to move in +z direction as shown in Figure 6(a), the friction is in –z direction and the total force applied to the shuttle magnet in z direction, F_{zT}, is given by:

$$F_{zT} = F_{zTm} - F_{fr} \tag{7}$$

When the shuttle magnet moves or tends to move in –z direction as shown in Figure 6(b), the friction is in +z direction and the total force applied to the shuttle magnet in z direction, F_{zT}, is given by:

$$F_{zT} = F_{zTm} + F_{fr} \tag{8}$$

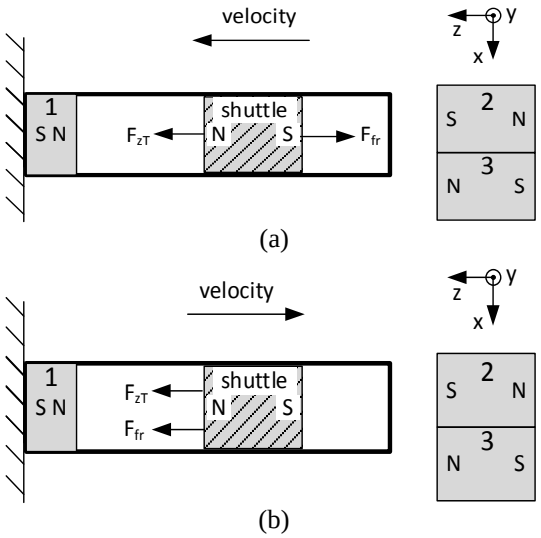

Figure 6. Total forces applied to the shuttle magnet (a) when it moves to the left (b) when it moves to the right.

3.3. Numerical analysis of movement of the shuttle magnet

In order to analyse movement of the shuttle magnet, a direct method is used to compute the solution in a finite number of steps. A small time interval is adopted between steps. In the remaining discussion in this paper, a subscripted n is used after parameter symbols to indicate the parameter at the *n*th step. Figure 7 illustrates parameters used in the numerical analysis.

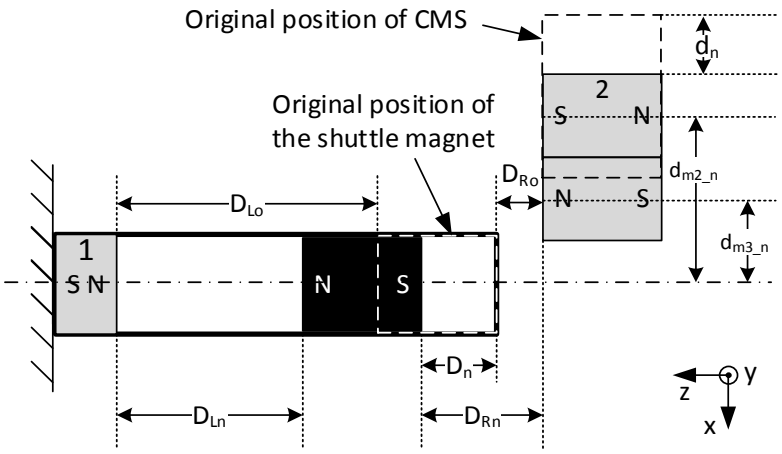

Figure 7. Illustration of parameters used in the numerical analysis.

In z direction, D_{Lo} and D_{Ro} is the initial distance between the shuttle magnet and magnet 1 and CMS respectively. D_{Ln} and D_{Rn} is the distance between the shuttle magnet and magnet 1 and CMS in the current step respectively. D_n is the displacement of shuttle magnet in the current step. Therefore, in z direction,

$$D_{Rn} = D_{R0} + D_{n-1} \tag{9}$$
$$D_{Ln} = D_{L0} - D_{n-1} \tag{10}$$

In x direction, d_{m2o} and d_{m3o} is the initial distance between centre of the shuttle magnet and centres of magnets 2 and 3 respectively. d_{m2_n} and d_{m3_n} is the distance between centre of the shuttle magnet and centres of magnets 2 and 3 in the current step respectively. d_n is displacement of CMS in the current step. Therefore, in x direction,

$$d_{m2\_n} = d_{m2o} - d_n \tag{11}$$
$$d_{m3\_n} = d_{m3o} - d_n \tag{12}$$

Therefore, total magnetic force applied to the shuttle magnet in z direction can be calculated using Eqs (1) and (2) as:

$$F_{zTm\_n} = F_{z2n}(D_L, 0, d_{m2\_n}) - F_{z1n}(0,0,D_L) - F_{z3n}(D_R, 0, d_{m3\_n}) \quad (13)$$

Total force applied to the shuttle magnet in x direction can be calculated using Eqs (1) and (3) to (5) as:

$$\text{Scenario 1: } F_{xT\_n} = G + F_{x2n}(D_{Rn}, 0, d_{m2\_n}) - F_{x3n}(D_{Rn}, 0, d_{m3\_n}) \quad (14)$$

$$\text{Scenario 2: } F_{xT\_n} = G + F_{x2n}(D_{Rn}, 0, d_{m2\_n}) + F_{x3n}(D_{Rn}, 0, d_{m3\_n}) \quad (15)$$

$$\text{Scenario 3: } F_{xT\_n} = G - F_{x2n}(D_{Rn}, 0, d_{m2\_n}) + F_{x3n}(D_{Rn}, 0, d_{m3\_n}) \quad (16)$$

Friction can thus be calculated according to Eq (6) as:

$$F_{fr\_n} = \mu \cdot F_{xT\_n} \quad (17)$$

where μ is coefficient of friction. If the shuttle magnet is still, i.e. its velocity in the last step, v_{n-1}, is 0, static coefficient is used. Otherwise, kinetic coefficient is used. If the shuttle magnet is still ($v_{n-1} = 0$) while friction force is greater than or equal to total magnetic force in z direction, the shuttle magnet cannot move and thus the total magnetic force applied to the shuttle magnet in z direction, F_{T_n}, is 0. Otherwise, F_{T_n} can be calculated by:

$$F_{T\_n} = F_{zT\_n} + sgn(v_{n-1}) \cdot F_{fr\_n} \quad (18)$$

where $sgn(v_{n-1})$ is the sign function that extracts the sign of v_{n-1}. Therefore, acceleration, a_n, velocity v_n and displacement, D_n, of the shuttle magnet in the current step can be calculated using fundamental equations of motion as:

$$a_n = \frac{F_{Tn}}{m} \quad (19)$$

$$v_n = v_{n-1} + a_n \cdot \Delta t \quad (20)$$

$$D_n = D_{n-1} + v_n \cdot \Delta t + \frac{1}{2} a_n \cdot \Delta t^2 \quad (21)$$

where Δt is the time interval between steps.

Figure 8 summarises the flow of the numerical analysis of the movement of the shuttle magnet presented in this subsection.

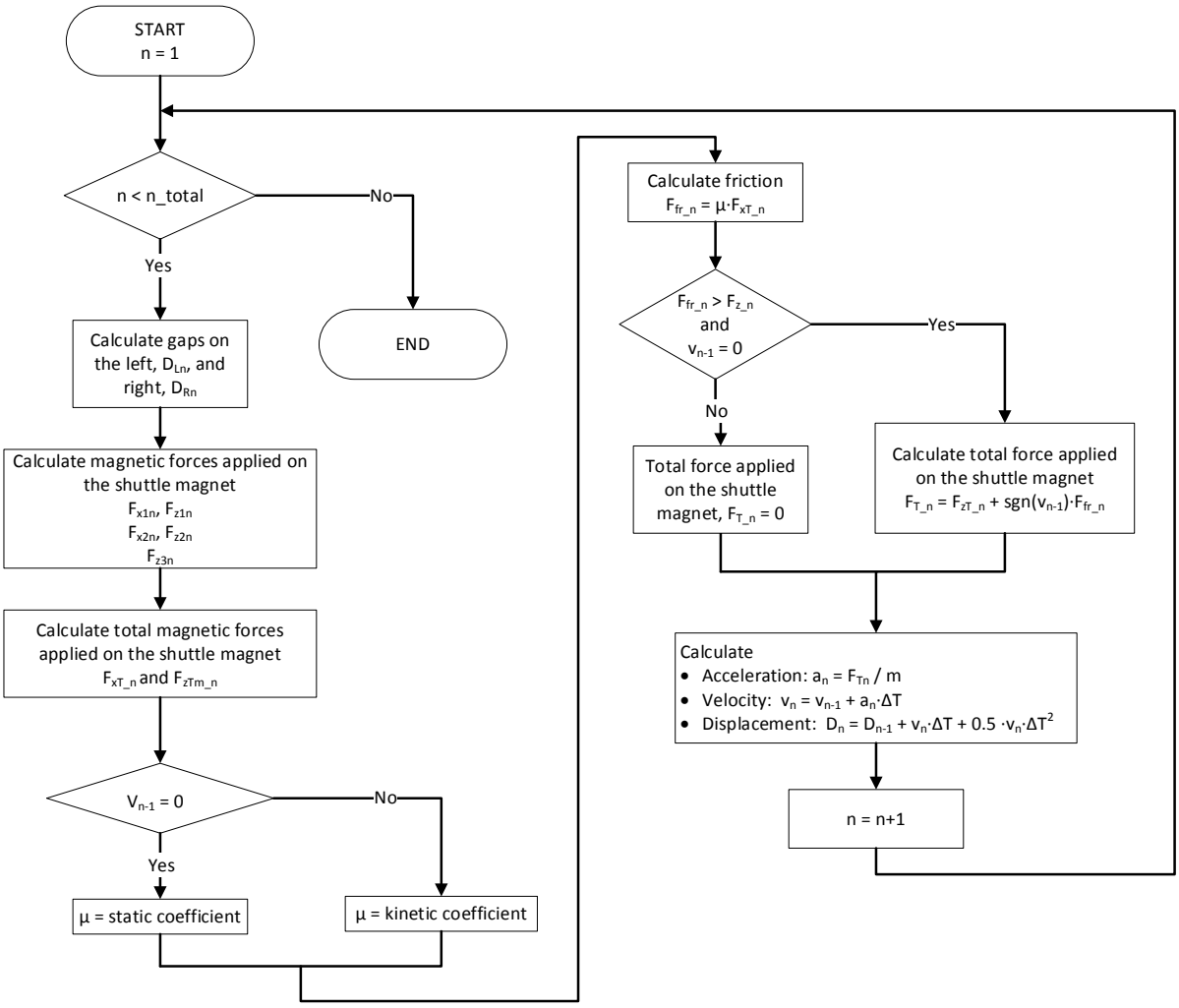

Figure 8. Flow of the numerical analysis of movement of the shuttle magnet.

3.4. Numerical analysis of open circuit voltage

According to Faraday's law of induction, electromotive force (EMF), i.e. voltage across a conductor is given by:

$$V = -N\frac{d\varphi}{dt} \tag{22}$$

where N is the number of turns of the conductor and $\frac{d\varphi}{dt}$ is the rate of change of the magnetic flux. Eq (22) can be written as:

$$V = -N\frac{d\varphi}{dt} = -N\frac{d\varphi}{dD}\cdot\frac{dD}{dt} \tag{23}$$

where $\frac{d\varphi}{dD}$ is the change of the magnetic flux with respect to change of magnet position and $\frac{dD}{dt}$ is the velocity of the magnet, v. Therefore,

$$V = -N\frac{d\varphi}{dD}\cdot v \tag{24}$$

In order to calculate induced voltage in a coil using numerical methods, the coil is divided into m sections along its length as shown in Figure 9. Length of each section is ΔD. Change of magnetic flux is determined in simulation using Maxwell 16.0. The magnet in the simulation has the same dimensions as the shuttle magnet. Figure 10(a)

shows the magnetic flux density around the magnet. Values of magnetic flux density was taken along the axis shown in Figure 10(a) at various positions and results are shown in Figure 10(b). Hence, change of magnetic flux with respect to magnet location can be calculated as:

$$\frac{\Delta\varphi}{\Delta D} = \frac{\Delta B \cdot A}{\Delta D} \tag{25}$$

where ΔB is the change of magnetic flux density for position change of ΔD and A is the cross area of the coil. In this case, ΔD is 1 mm and the average diameter of the coil is 19 mm, thus A is 2.84×10^{-4} m^2. Figure 10(c) shows the simulation results of change of magnetic flux with respect to magnet location.

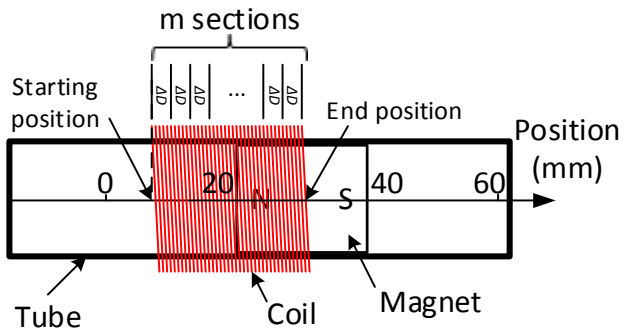

Figure 9. Configuration of the magnet and coil.

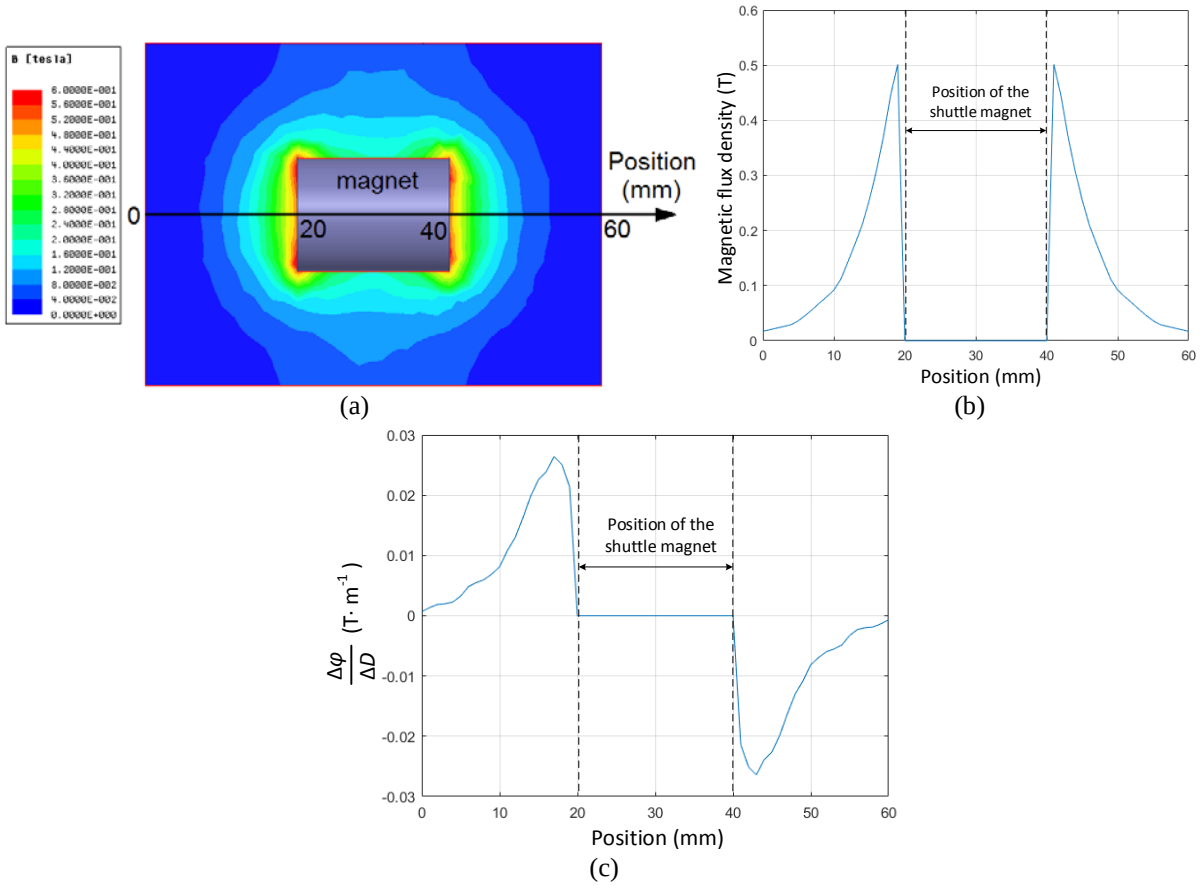

Figure 10. Simulation of magnetic flux density in Maxwell 16.0. (a) Magnetic field distribution (b) magnetic flux density at various locations (c) change of magnetic flux with respect to magnet location.

Depending on the position of the coil with respect to the shuttle magnet, corresponding $\frac{\Delta\varphi}{\Delta D}$ is used to calculate the induced voltage at the *n*th step, V_n, as:

$$V_n = -\frac{N}{m} \cdot \sum_{i=1}^{m} \left(\frac{\Delta\varphi}{\Delta D}\right)_i \cdot v_n \tag{26}$$

where $\left(\frac{\Delta\varphi}{\Delta D}\right)_1$ and $\left(\frac{\Delta\varphi}{\Delta D}\right)_m$ corresponds to the change of flux at the starting and end positions respectively as shown in Figure 9. It is worth mentioning that the induced voltage calculated in this case is the open circuit voltage, which means there is no closed loop current. Thus, current induced magnetic force exerted to the shuttle magnet is not considered in this study.

4. Verification of the numerical analysis

4.1. Measurement of coefficient of friction

Coefficient of static friction between the shuttle magnet and the tube was measured using tilt plane method as shown in Figure 11. The tube holding the shuttle magnet was placed on a tilted plane. The angle of tilt was increased gradually until the shuttle magnet began to slide. This angle, α, also called friction angle, was found to be 34.5°. Tangent of the friction is the coefficient of static friction μs, i.e.

$$\mu_s = \frac{F_{frs}}{F_N} = \tan\alpha = 0.69 \tag{27}$$

where F_{frs} is the static friction and F_N is the force perpendicular to the contact surface. Coefficient of kinetic friction was estimated as 0.5 according to literature [16].

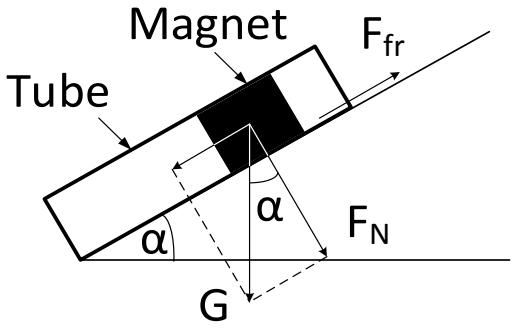

Figure 11. Measurement of coefficient of static friction.

4.2. Initial conditions

Initial conditions for both experimental setup and the numerical analysis are summarised in Table 1.Two scenarios were considered to verified the numerical model, i.e. D_{Lo} = 0.08 m and 0.072 m. Details of these parameters have been illustrated in Figure 7.

Table 1. Summary of initial conditions.

CMS displacement, d_0 (m)	0
Shuttle magnet displacement, D_0 (m)	0
Shuttle magnet velocity, v_0 (m·s^{-1})	0
Shuttle magnet acceleration, a_0 (m·s^{-2})	0
Distance between the shuttle magnet and magnet 1, D_{Lo} (m)	0.08 and 0.072
Distance between the shuttle magnet and CMS, D_{Ro} (m)	0.017
Distance between centre of the shuttle magnet and centre of magnet 2, d_{m2o} (m)	0.0195
Distance between centre of the shuttle magnet and centre of magnet 3, d_{m3o} (m)	0.0115

4.3. Excitation

Excitation was applied as displacement of CMS along x axis. Profile of such displacement within one excitation cycle is shown in Figure 12. The excitation is divided into four stages, i.e. 1. excitation, 2. hold, 3. release and 4. idle. In the excitation stage, the CMS moves from the initial position by 31 mm in +x direction to the end position within 0.1s. In the hold stage, the CMS remain at the end position for 0.4 s. In the release stage, the CMS moves back to the initial position within 0.1 s. The CMS then remains at the initial position for another 0.4 s in the idle stage.

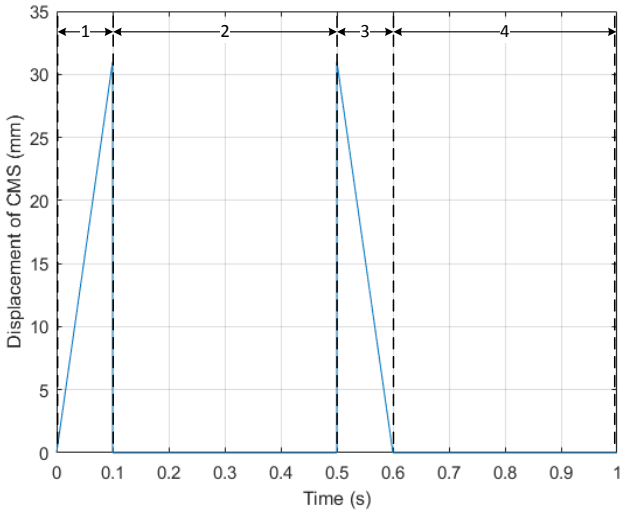

Figure 12. Displacement profile of CMS within one excitation cycle.

4.4. Experimental

A prototype was manufactured for testing as shown in Figure 13. The plastic tube is 80 mm long. Rubber end stops are placed on both end of the tube to avoid collision between magnets. All magnets used here are made of NdFeB-38. The shuttle magnet is a 20 mm long cylinder magnet with a diameter of 15 mm. The fixed magnet on the left of the tube is a 15 mm × 15 mm × 5 mm (m) rectangular. The two bar magnets in the CMS have dimensions of 20 mm × 10 mm × 8 mm (m). (m) notates the magnetization of the magnets. The coil is wound using 75 µm thick copper enamel wire. It has around 500 turns and a resistance of 180Ω. All the supporting structures are made of 3D printed PLA. In the experiment, the CMS was driven by a stepper motor and it moved following the profile described in section 4.3. The reason of using a stepper motor instead of actual footsteps to drive the structure in this test is that footsteps are random in amplitude and frequency while the stepper motor can provide a controlled excitation with a particular frequency and amplitude. This can provide more accurate results to verify the numerical model. However, in practical application, this energy harvesting structure will still be driven by external excitations such as footsteps.

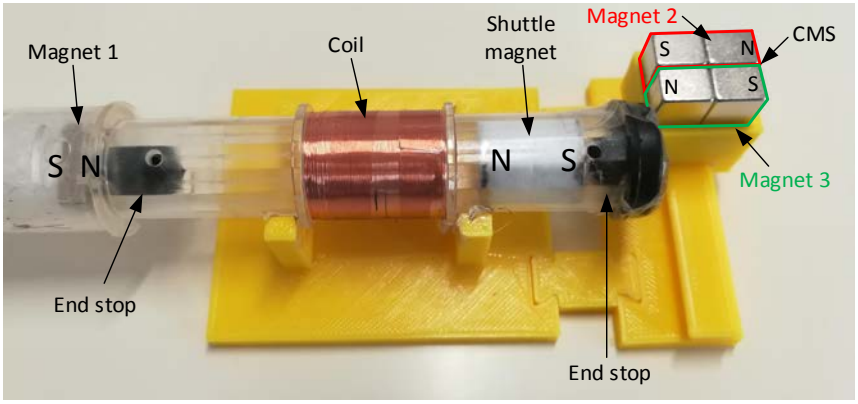

Figure 13. Photo of the testing prototype (stepper motor not shown).

4.5. Results

The numerical analysis was implemented in Matlab. The interval between steps are 100 µs. Two scenarios were considered in this study, i.e. D_{Lo} = 0.08 m and D_{Lo} = 0.072 m.

4.5.1. Scenario 1 (D_{Lo} = 0.08 m). Figure 14 and 15 present numerical results of forces exerted to the shuttle magnets as well as displacement and velocity of the shuttle magnets at different stages when D_{Lo} = 0.08 m respectively. There are seven critical moments within one excitation cycle which are marked A to G in Figure 14 and 15. When the CMS starts moving, although various magnetic forces are exerted to the shuttle magnet, the total magnetic force is smaller than static friction force. Therefore, the shuttle magnet remains static. At moment A, total magnetic force becomes greater than static friction force, thus the shuttle magnet starts moving. As total force is positive, the shuttle magnet accelerates towards +z direction. At moment B, the total force becomes negative, which means that the shuttle magnet starts decelerating. However, as the velocity is still positive, the shuttle magnet keeps traveling in +z direction. At moment C, the velocity of the shuttle magnet becomes negative, which means it starts moving in –z direction. At moment D, the total force is positive again so the velocity increases. As the velocity remains negative, the shuttle magnet continues travelling in –z direction. At moment E, both total force and velocity becomes zero, which means the shuttle magnet stops moving. When CMS moves back to the initial position, i.e. moment F, both total force and velocity are negative so the shuttle magnet moves back to its initial position at moment G and then the velocity becomes zero. This completes one excitation cycle. Figure 16 compares open circuit voltage across the coil measured in experiment and calculated in numerical analysis when D_{Lo} = 0.08 m. It was found that the two results agree with each other, which verifies the numerical analysis model presented in section 3. The ripple on the output voltage found in the experiment (highlighted in Figure 16) is caused by the impact between the shuttle magnet and the end stop. This is beyond the scope of this paper so is not considered in the numerical model.

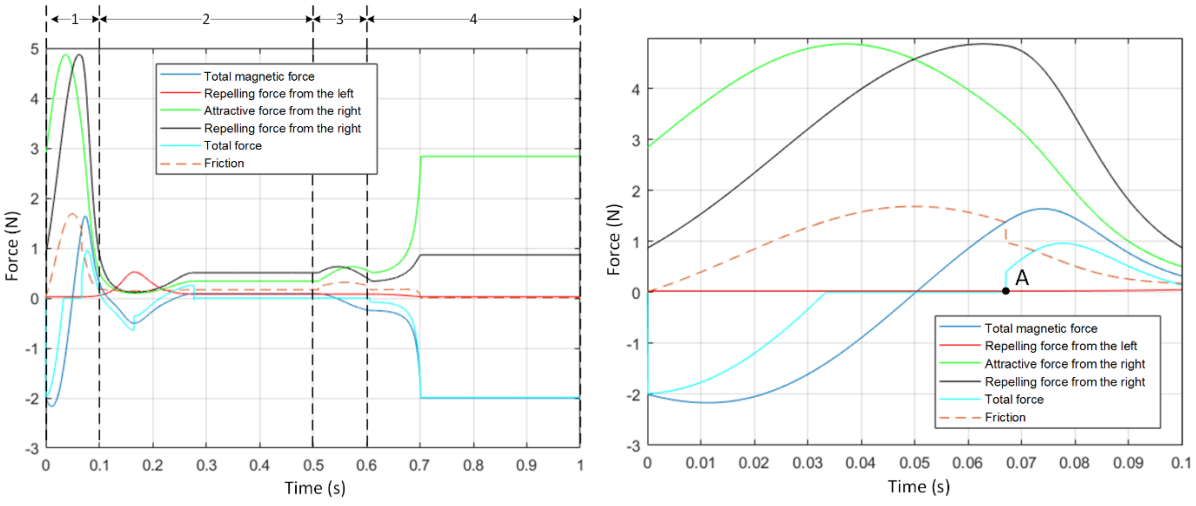

(a) (b)

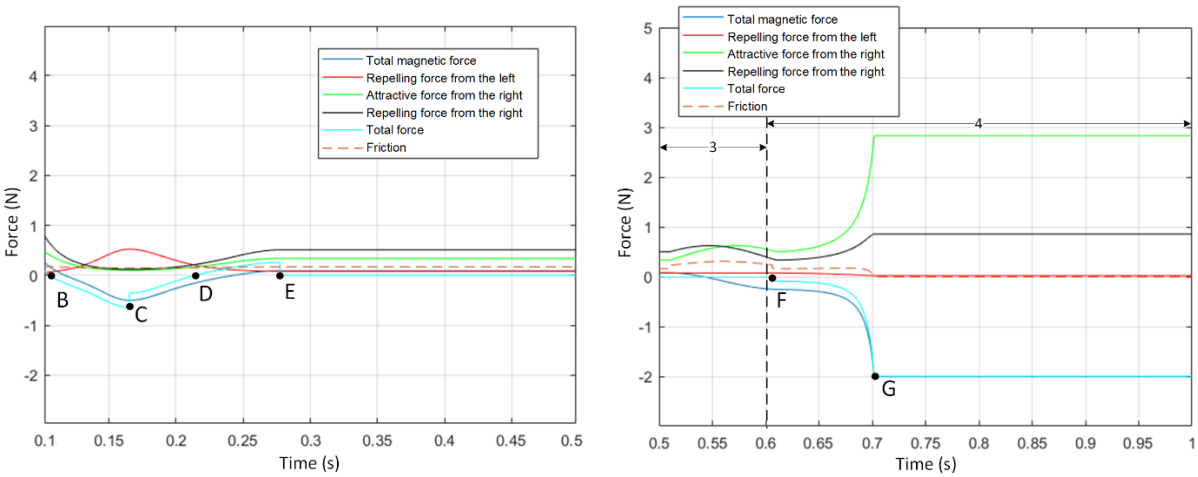

(c) (d)

Figure 14. Force exerted to the shuttle magnet in z direction when D_{Lo} = 0.08 m (a) for the entire cycle (b) in excitation stage (c) in hold stage (d) in release (3) and idle (4) stages.

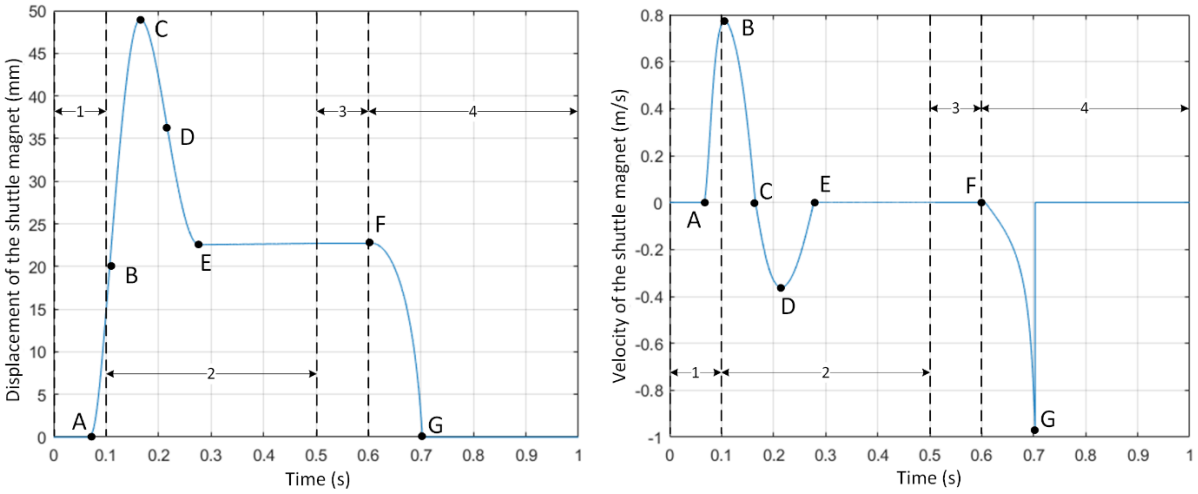

(a) (b)

Figure 15. Numerical results of (a) displacement and (b) velocity of the shuttle magnet when D_{Lo} = 0.08 m.

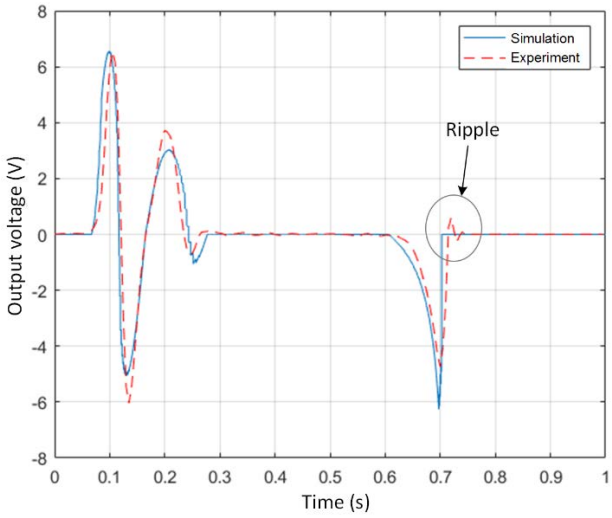

Figure 16. Comparison of open circuit voltage across the coil measured in experiment and calculated in numerical analysis when D_{Lo} = 0.08 m.

4.5.2. Scenario 2 (D_{Lo} = 0.072 m). A second scenario when D_{Lo} = 0.072 m is also analysed to compare with scenario 1. As D_{Lo} becomes shorter, the repelling force from magnet 1 increases, which has big impact on performance of the structure. Figures 17 and 18 present numerical results of forces exerted to the shuttle magnets as well as displacement and velocity of the shuttle magnets at different stages when D_{Lo} = 0.072 m respectively. Critical moments within one excitation cycle are marked A to I in Figures 17 and 18. The start of the operation (A to E) is similar to that in scenario 1. However, although velocity of the shuttle magnet becomes zero at moment E, total force is still positive. This means that the shuttle magnet starts accelerating in +z direction. At moment F, total force becomes negative and the shuttle magnets start decelerating in +z direction. At both total force and velocity becomes zero at moment G, the shuttle magnet stops. When CMS moves back to the initial position in the release stage, total magnet force exceeds static friction force at moment H so the shuttle magnet moves back to its initial position at moment I and stops. This completes one excitation cycle. Figure 19 compares open circuit voltage across the coil measured in experiment and calculated in numerical analysis when D_{Lo} = 0.072 m. Again, the two results agree with each other. The ripple on the output voltage caused by the impact between the shuttle magnet and the end stop in this scenario is found to be more apparent than that in scenario 1. This is because the impact is stronger as the repelling force from magnet 1 is greater.

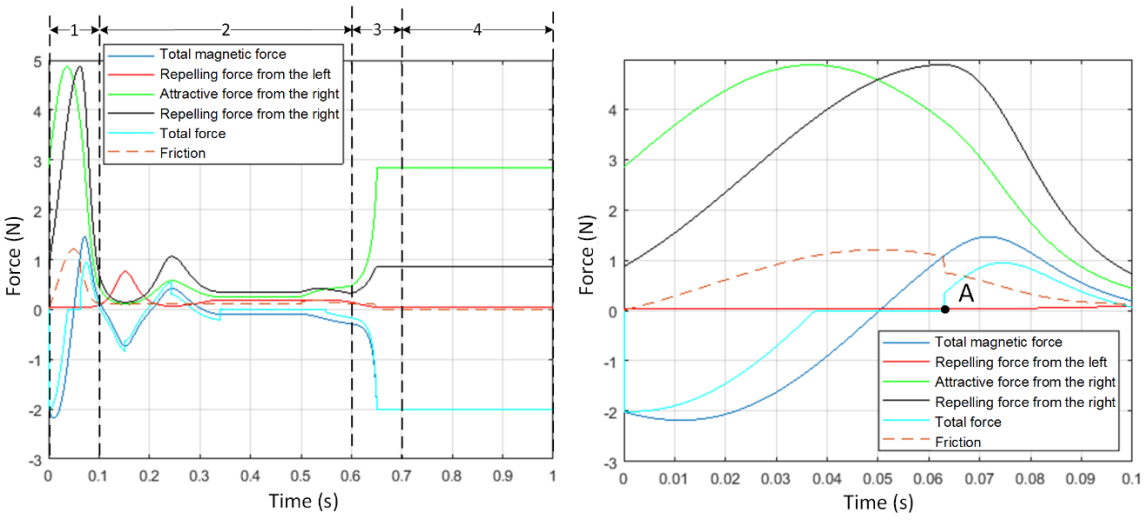

(a) (b)

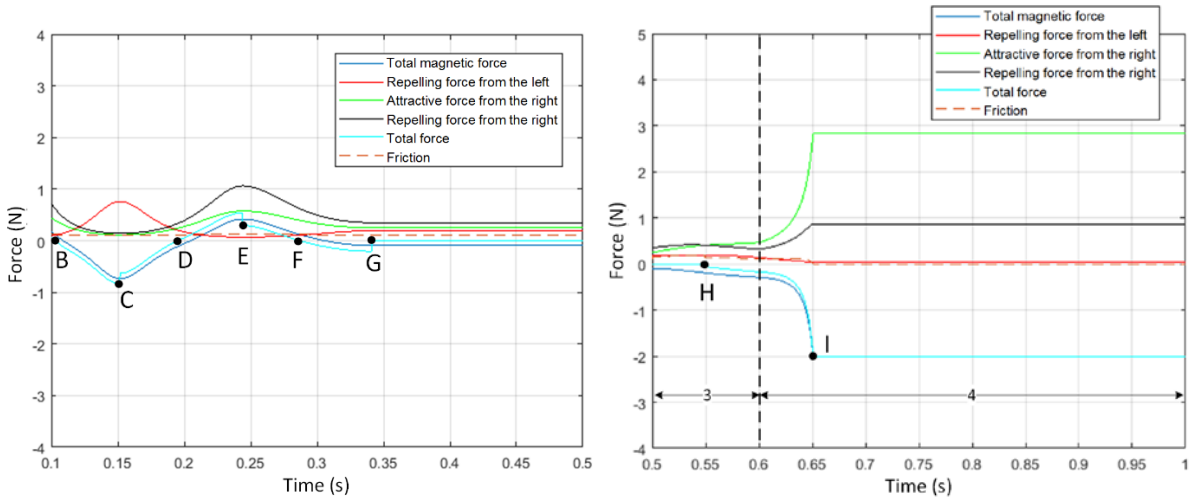

(c) (d)

Figure 17. Force exerted to the shuttle magnet in z direction when D_{Lo} = 0.072 m (a) for the entire cycle (b) in excitation stage (c) in hold stage (d) in release (3) and idle (4) stages.

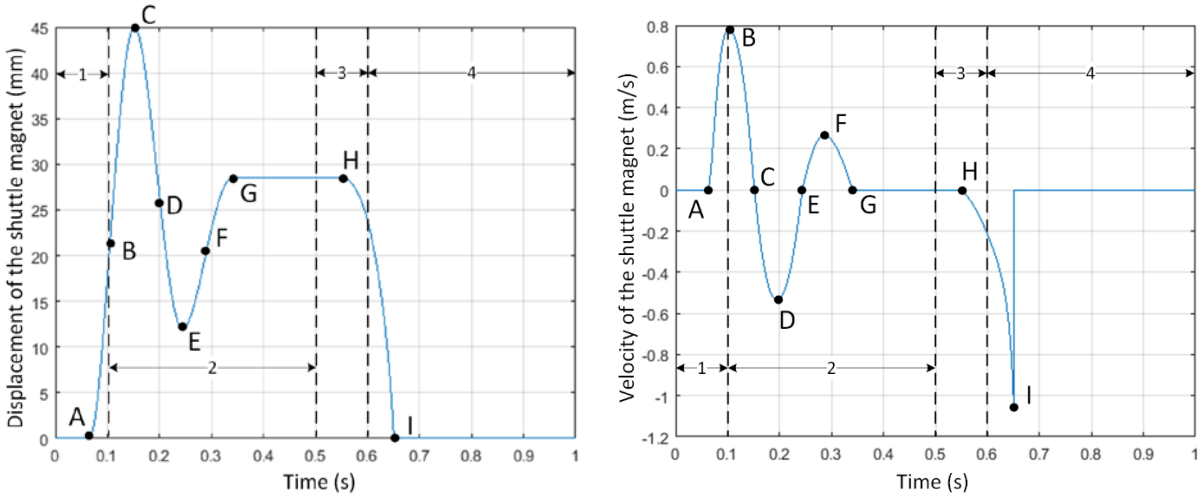

(a) (b)

Figure 18. Numerical results of (a) displacement and (b) velocity of the shuttle magnet when D_{Lo} = 0.072 m.

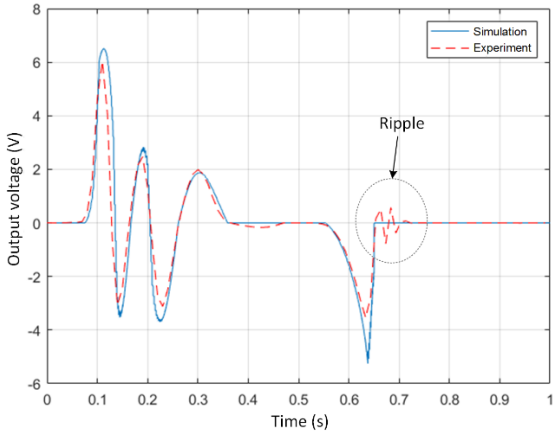

Figure 19. Comparison of open circuit voltage across the coil measured in experiment and calculated in numerical analysis when D_{Lo} = 0.072 m.

4.6. Discussions

Experimental results obtained in both scenarios have verified that the numerical analysis model presented in this paper is viable and can be used to predict performance of the proposed structure accurately. It has demonstrated that the initial distance between magnet 1 and the shuttle magnet, D_{Lo}, can change oscillation pattern of the shuttle magnet significantly. As D_{Lo} becomes smaller, more dramatic oscillation can be triggered. In addition, initial position of magnet 1 also affects the maximum displacement of the shuttle magnet. As D_{Lo} becomes lower, the repelling force from magnet 1 is greater. Therefore, it provides more resistance to the shuttle magnet thus the maximum displacement reduces. According to numerical analysis, the maximum displacement of the shuttle magnet in scenario 1 is 48.98 mm compared to 44.97 mm in scenario 2. It is also found that when D_{Lo} reduces below 18mm, the repelling force from magnet 1 becomes so large that the shuttle magnet cannot move at all.

Numerical analysis also suggests that the coefficient of friction plays an important part of oscillation of the shuttle magnet. If the coefficient of kinetic friction was reduced to 0.2 in scenario 2, both oscillation of the shuttle magnet and output open circuit voltage would last longer as shown in Figure 20, which potentially means more energy could be generated under the same pulse excitation.

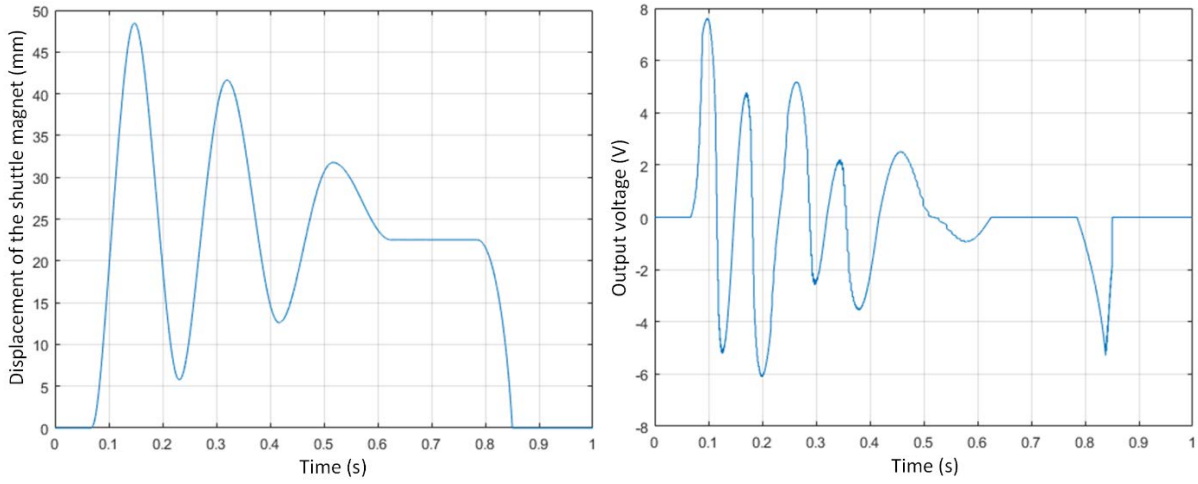

(a) (b)

Figure 20. Numerical results of (a) displacement of the shuttle magnet and (b) open circuit output voltage when D_{Lo} = 0.072 m and coefficient of kinetic friction is 0.2.

Energy harvesting capability of an energy harvester using the proposed structure was demonstrated in [14] where more details can be found. The prototype was tested under a series of footsteps of 1 Hz. Experimentally, an average energy of 2.8 mJ, i.e. an average energy of 2.8 mW, was generated under footsteps of 1 Hz. Given the total device volume of 66 cm^3, the power density of the energy harvester is 42.4 $\mu W \cdot cm^{-3}$. The value is comparable to the two highly rated electromagnetic footstep energy harvesters presented in [10], which have power density of 40 and 86 $\mu W \cdot cm^{-3}$ respectively.

5. Conclusions

This paper presents a numerical analysis model of an electromagnetic energy harvester that is driven by multiple magnetic forces under pulse excitation. The model correlates analytical calculation of magnetic forces and simulation results of magnetic field. Operation of the structure was then analysed using fundamental equations of motion in the time domain. In the two example scenarios presented in this paper, both experimental results agreed with respective numerical results, which proves that the model is valid.

For the proposed mechanism that consists of a tube with magnets on both ends and a shuttle magnet moving inside, initial positions of the end magnets with respect to the shuttle magnet are crucial to the performance of the energy harvester. It was found that as the initial distance between the end magnet and the shuttle magnet gets closer, oscillation of the shuttle magnet is likely to last longer while its amplitude reduces. This is due to increased magnetic force between them. The shuttle magnet can stop oscillate when such distance reduces below a threshold

value. One potential method to improve performance of the proposed mechanism is to reduce the friction between the shuttle magnet and the tube. If this can be achieved, oscillation of the shuttle magnet will have larger amplitude and last longer.

In addition, the proposed numerical method mainly focuses on the mechanical domain. Therefore, only open circuit voltage can be estimated as this is the case when no electrical load is connected. Future improvement can be made by linking the electrical domain with the mechanical domain and considering effects of electrical load on the mechanical performance of the shuttle magnet.

The mechanism investigated in this paper is suitable for energy harvesting from pulse excitation such as footsteps as demonstrated in [14]. To achieve this, it can be adapted for either integration with shoes or being embedded underneath the floor. It can also be potentially used for energy harvesting in environment where excitation has low frequency and large amplitude, such as wave energy harvesting. With the successful development of the numerical analysis model, the mechanism can be optimised numerically to improve its performance. Furthermore, the proposed concept of numerical analysis can be adapted so that it can be used to model more complex electromechanical structures.

Reference

[1] Choi Y-M, Lee M G and Jeon Y 2017 Wearable Biomechanical Energy Harvesting Technologies *Energies* **10(10)** 1483.

[2] Xin y, Li X, Tian H, Guo C, Qian C, Wang S and Wang C 2016 Shoes-equipped piezoelectric transducer for energy harvesting: A brief review *Ferroelectrics* **493(1)** 12-24.

[3] Li H, Tian C and Deng Z D 2014 Energy harvesting from low frequency applications using piezoelectric materials *Applied Physics Reviews* **1** 041301.

[4] Luo Z, Zhu D and Beeby S P 2015 Multilayer ferroelectret-based energy harvesting insole, *Journal of Physics: Conference Series*, **660 (1)**.

[5] Pavegen Ltd, available from: http://www.pavegen.com [Accessed 21st June 2018].

[6] Beeby S P, Tudor M J and White N M 2006 Energy harvesting vibration sources for microsystems pplications *Meas. Sci. Technol.* **17** pp 175–195.

[7] Paradiso J A and Starner T 2005 Energy scavenging for mobile and wireless electronics *IEEE Pervasive Comput.* **4** 18–27.

[8] Palosaari J, Leinonen M, Juuti J, Hannu J and Jantunen H 2012 Energy harvesting with a cymbal type piezoelectric transducer from low frequency compression *J Electroceram* **28** 214–219.

[9] Palosaari J, Leinonen M, Juuti J, Hannu J and Jantunen H 2014 Piezoelectric circular diaphragm with mechanically induced pre-stress for energy harvesting *Smart Mater. Struct.* **23** 085025.

[10] Ylli K, Hoffmann D, Willmann A, Becker P, Folkmer B and Manoli Y 2015 Energy harvesting from human motion: exploiting swing and shock excitations *Smart Mater. Struct.* **24(2)** 025029.

[11] Tang Q C, Yang Y L and Li X 2011 Bi-stable frequency up-conversion piezoelectric energy harvester driven by non-contact magnetic repulsion *Smart Mater. Struct.* **20** 125011.

[12] Liu H, Lee C, Kobayashi T, Tay C J and Quan C 2011 Piezoelectric MEMS-based wideband energy harvesting systems using a frequency-up-conversion cantilever stopper *Sensors and Actuators A: Physical* **186** 242–248.

[13] Xu Z , Wang W , Xie J, Xu Z, Zhou M and Yang H 2017 An Impact-Based Frequency Up-Converting Hybrid Vibration Energy Harvester for Low Frequency Application *Energies* **10(11)** 1761.

[14] Zhu D and L Evans 2017 An electromagnetic energy harvester capable of frequency up-conversion and amplitude amplification under pulse excitation *Proc. PowerMEMS 2017, Kanazawa, Japan, 11th - 14th Nov 2017*.

[15] Akoun G and Yonnet J P 1984 3D analytical calculation of the forces exerted between two cuboidal magnets *IEEE Transactions on Magnetics* **20(5)** 1962-4.

[16] Engineers Edge LLC (2018b) Coefficient of Friction Equation and Table Chart. Engineers Edge, available from: https://www.engineersedge.com/coeffients_of_friction.htm [Accessed 21st June 2018].